

## Electronic Supplementary Information

### From Covalent Triazine-based Framework to N-doped Porous Carbon/Reduced Graphene Oxide Nanosheets: Efficient Electrocatalysts for Oxygen Reduction

Long Jiao, Yingli Hu, Huanxin Ju, Chunde Wang, Min-Rui Gao, Qing yang, Junfa Zhu, Shuhong Yu, and Hai-Long Jiang\*

*L. Jiao, Y. Hu, C. Wang, Prof. M.-R. Gao, Prof. Q. Yang, Prof. S.-H. Yu, Prof. H.-L. Jiang*

*Hefei National Laboratory for Physical Sciences at the Microscale, CAS Key Laboratory of Soft Matter Chemistry, Collaborative Innovation Center of Suzhou Nano Science and Technology, Department of Chemistry, University of Science and Technology of China, Hefei, Anhui 230026, P.R. China*

*Dr. H. Ju, Prof. J. Zhu*

*National Synchrotron Radiation Laboratory, University of Science and Technology of China, Hefei, Anhui 230029, P. R. China*

\*To whom correspondence should be addressed.

E-mail: [jianglab@ustc.edu.cn](mailto:jianglab@ustc.edu.cn)

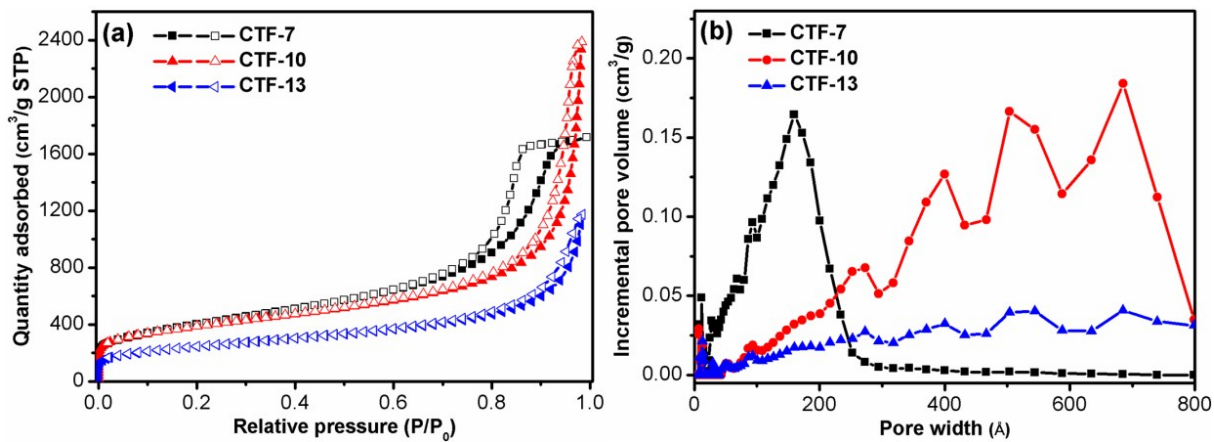


**Fig. S1.** (a)  $\text{N}_2$  sorption isotherms at 77 K for CTFs obtained on the basis of different mass ratios of DCBP and  $\text{ZnCl}_2$  and (b) the corresponding pore size distributions calculated by the DFT model.

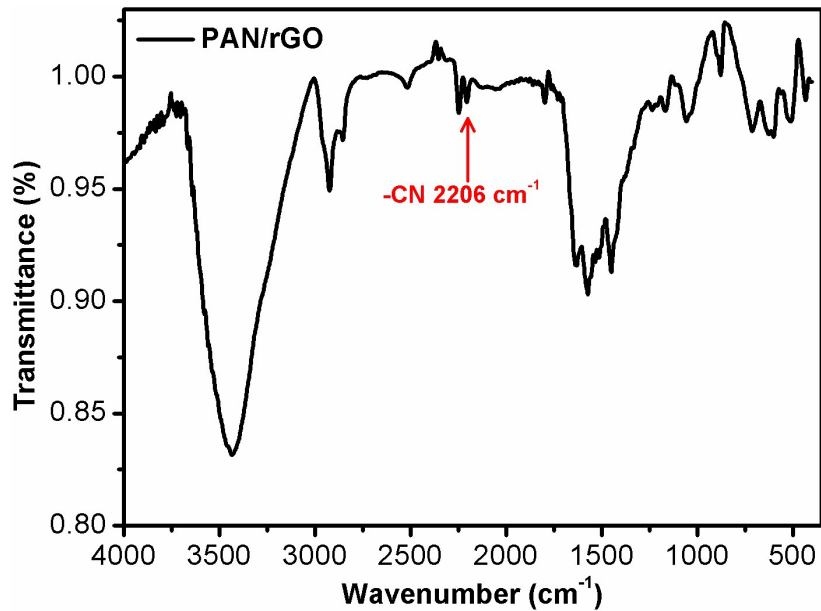


**Fig. S2.** FT-IR spectrum of PAN/rGO. A vibration at *ca.* 2206  $\text{cm}^{-1}$  is detected that can be assigned to the -CN stretching vibration, illustrating the successful fabrication of PAN on rGO.

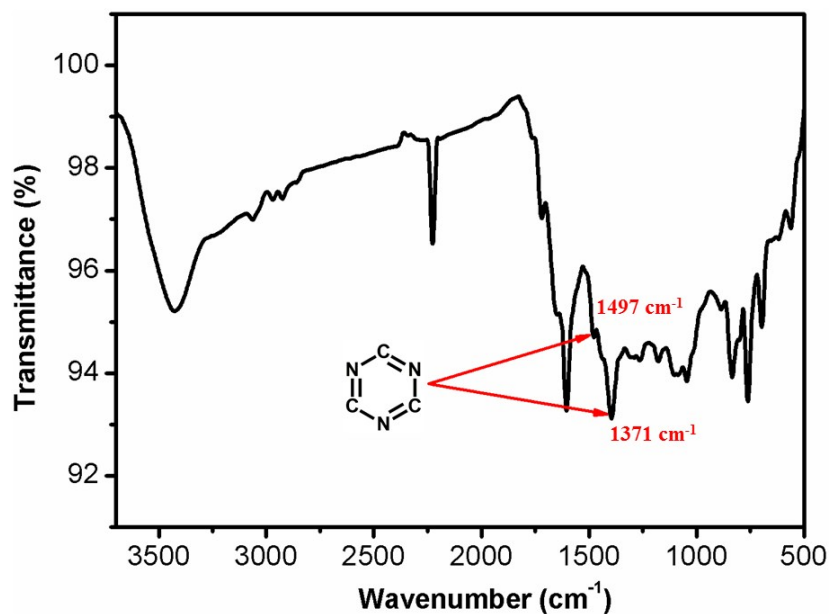


**Fig. S3.** FT-IR spectrum indicating the formation of CTF during polymerization process. The formation of triazine rings is supported by the two strong absorption bands at 1497 and  $1371 \text{ cm}^{-1}$ , revealing the aromatic C–N stretching and “breathing” modes in the triazine unit, respectively.

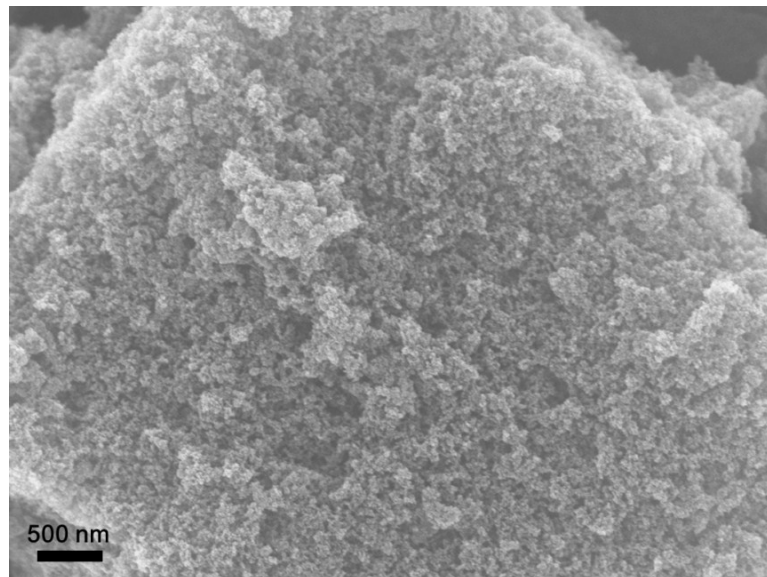


**Fig. S4.** SEM image of NHC-950.

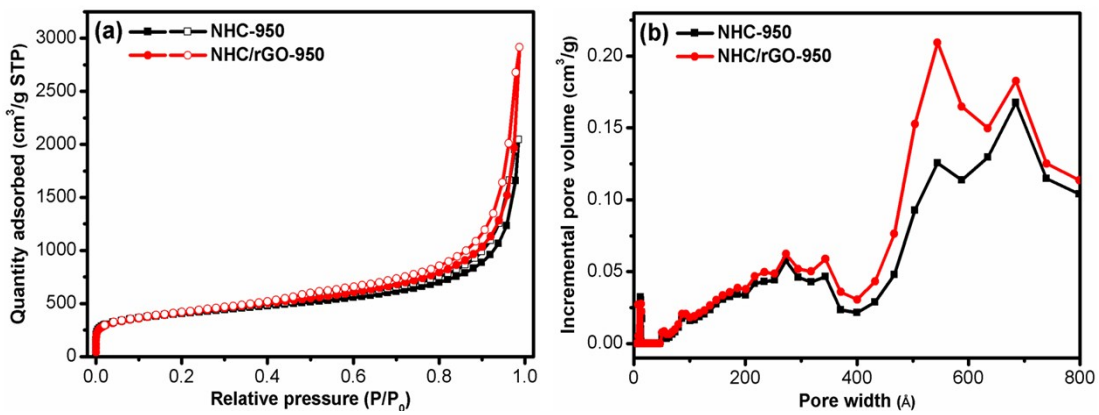


**Fig. S5.** (a)  $N_2$  sorption isotherms for NHC-950 and NHC/rGO-950 at 77 K and (b) the corresponding pore size distributions calculated by the DFT model.

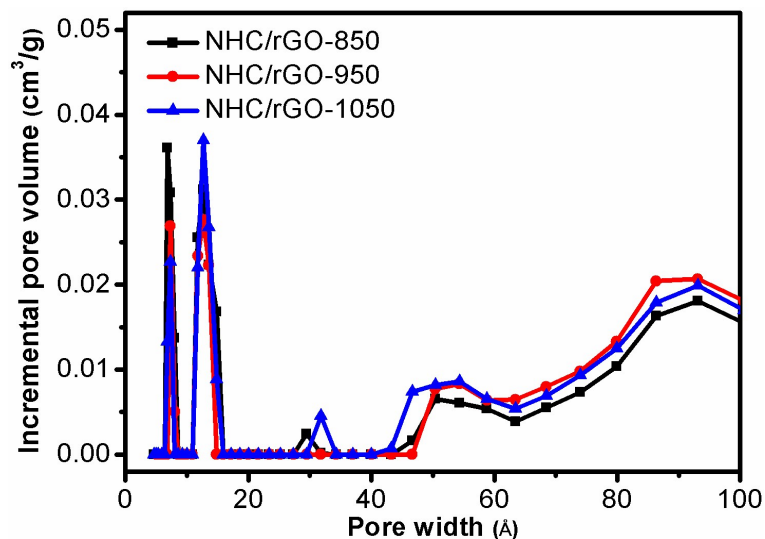


**Fig. S6.** The pore size distributions below 10 nm for NHC/rGO-T at 77 K calculated by the DFT model.

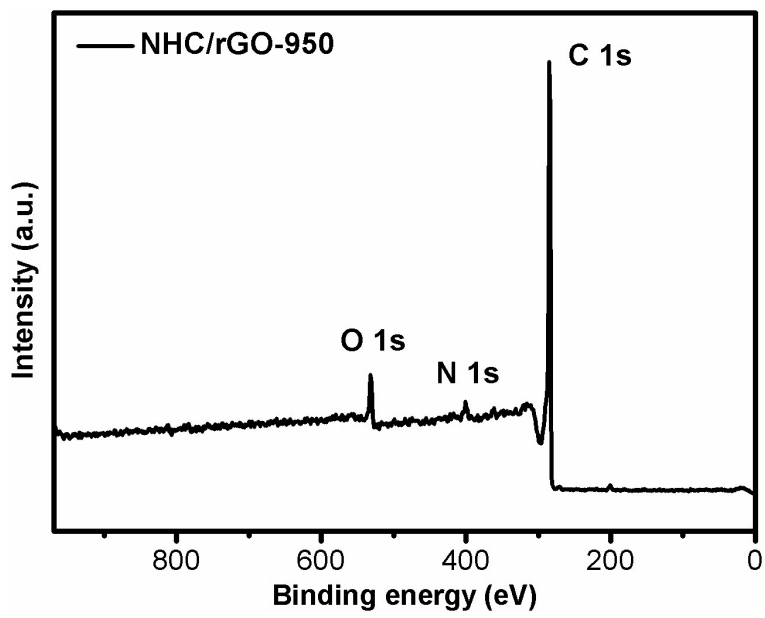


**Fig. S7.** XPS survey spectrum of NHC/rGO-950.

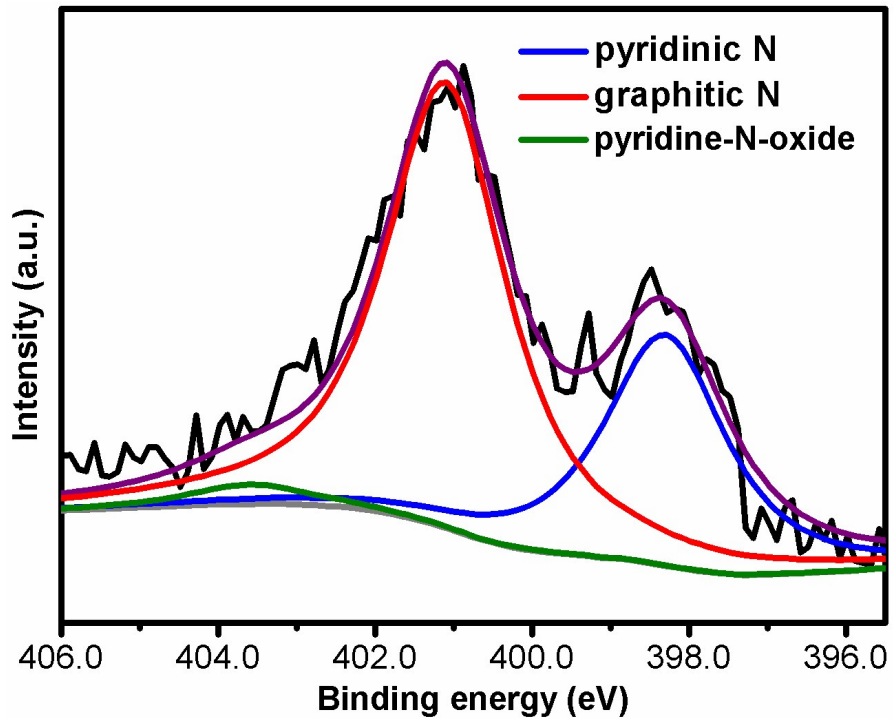


**Fig. S8.** The high-resolution N1s XPS spectrum of NHC/rGO-850.

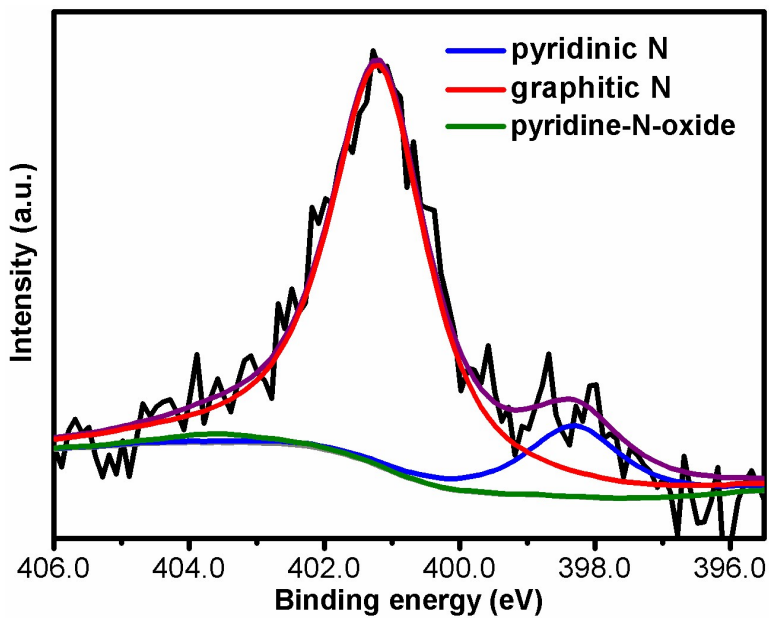


**Fig. S9.** The high-resolution N1s XPS spectrum of NHC/rGO-1050.

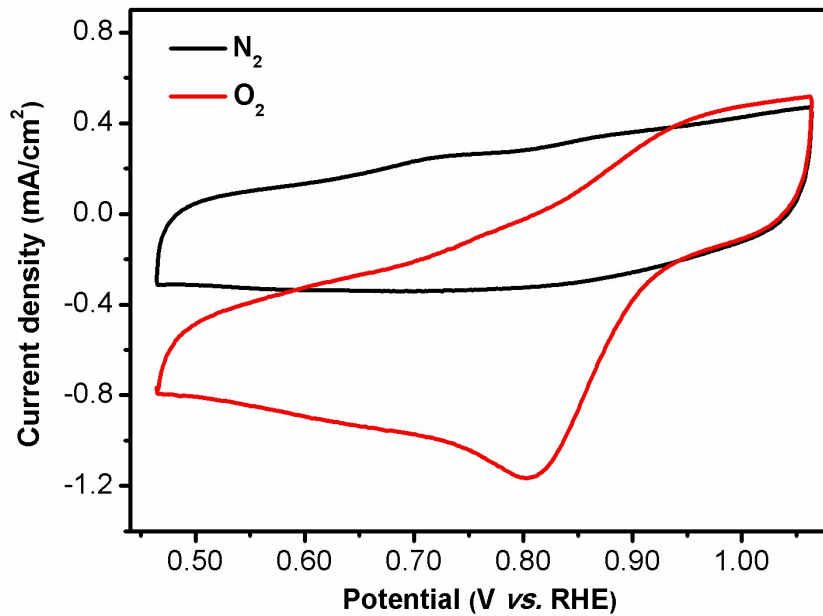


**Fig. S10.** CV curves of Pt/C in  $N_2$  and  $O_2$ -saturated 0.1 M KOH solution.

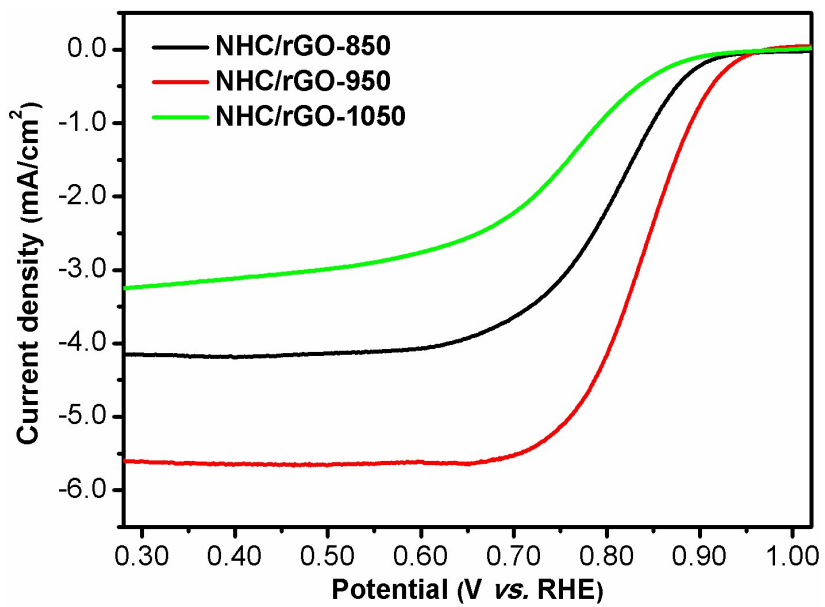


**Fig. S11.** Electrochemical ORR activity evaluation for NHC/rGO-T (T = 850, 950 and 1050) obtained at different pyrolysis temperatures in 0.1 M KOH solution.

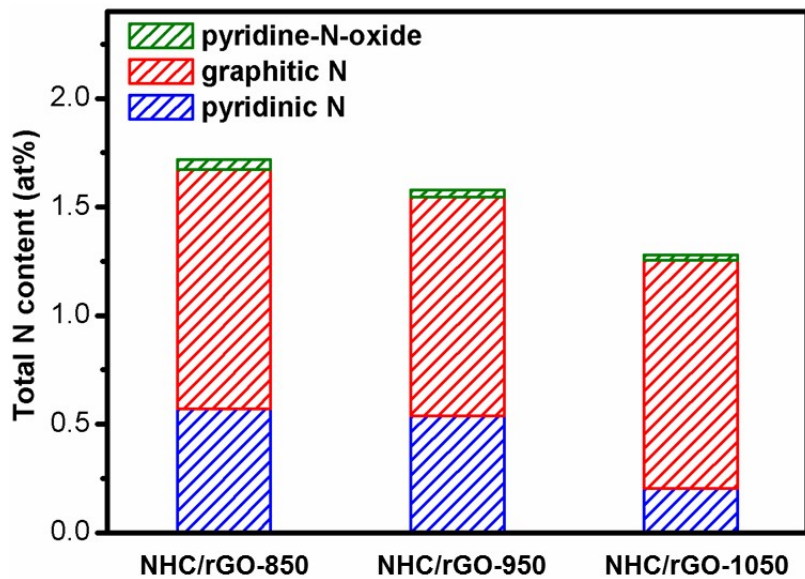


**Fig. S12.** Summary of the different nitrogen levels in NHC/rGO-T.

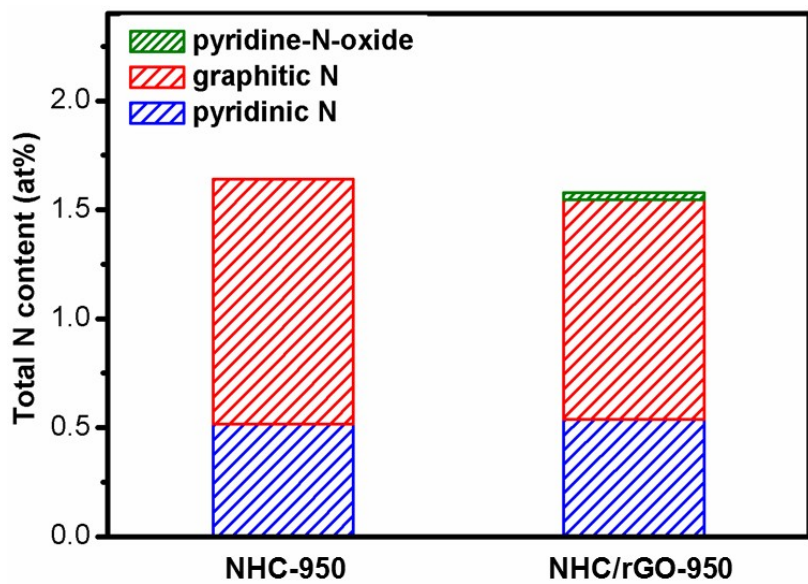


**Fig. S13.** Summary of the different nitrogen levels in NHC/rGO-950 and NHC-950.

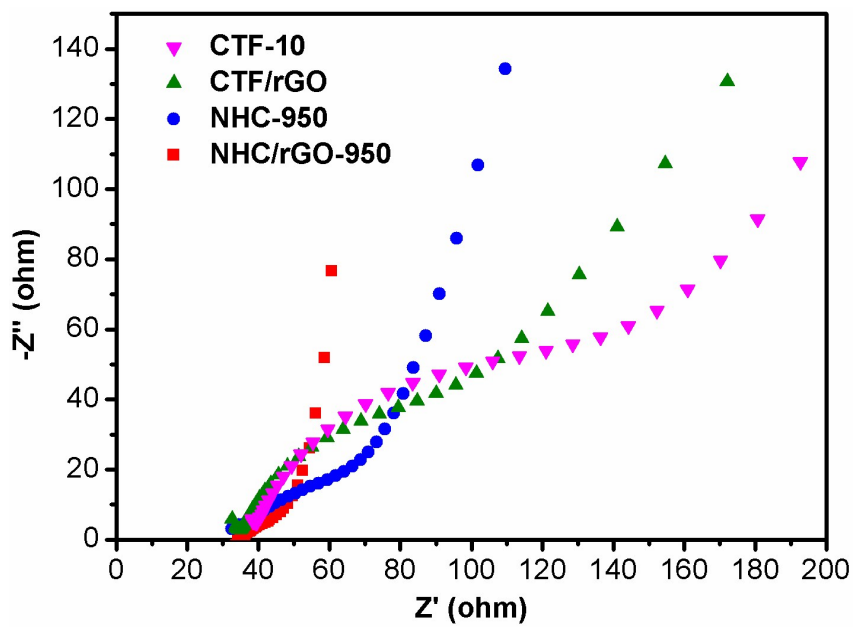


**Fig. S14.** Nyquist plots of electrochemical impedance spectra for different samples in 0.1 M KOH.

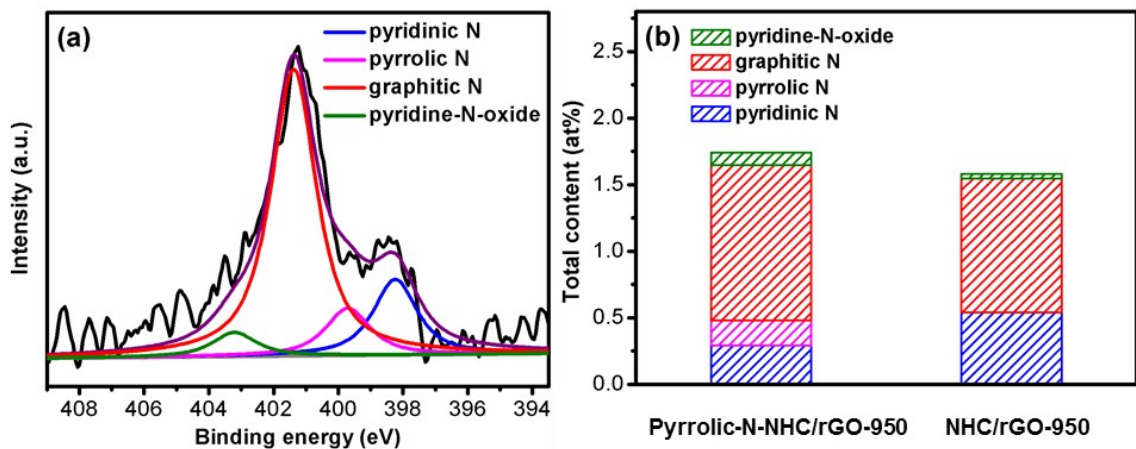


**Fig. S15.** (a)The high-resolution N1s XPS spectrum and (b) summary of the different nitrogen levels of pyrrolic-N-NHC/rGO-950.

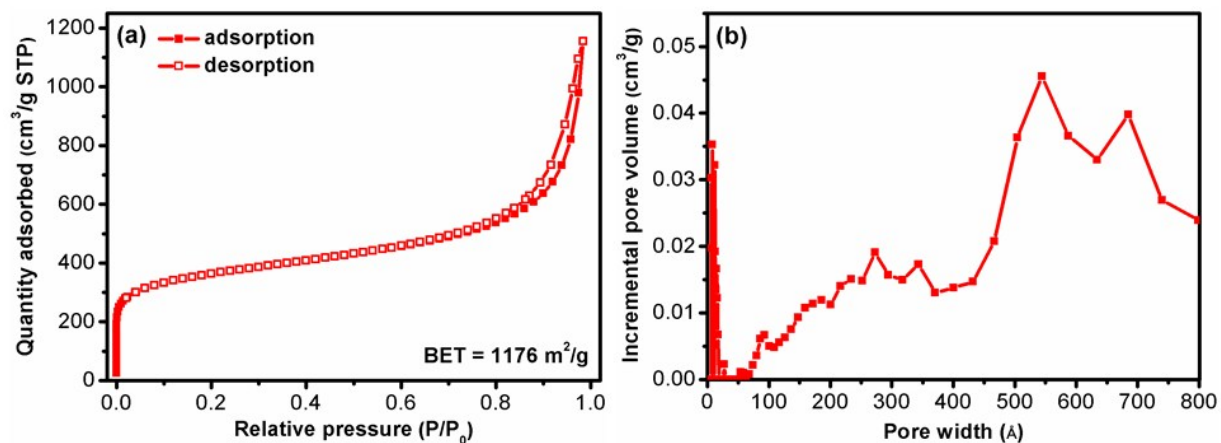


**Fig. S16.** (a) N<sub>2</sub> sorption isotherms for pyrrolic-N-NHC/rGO-950 at 77 K and (b) the corresponding pore size distributions calculated by the DFT model.

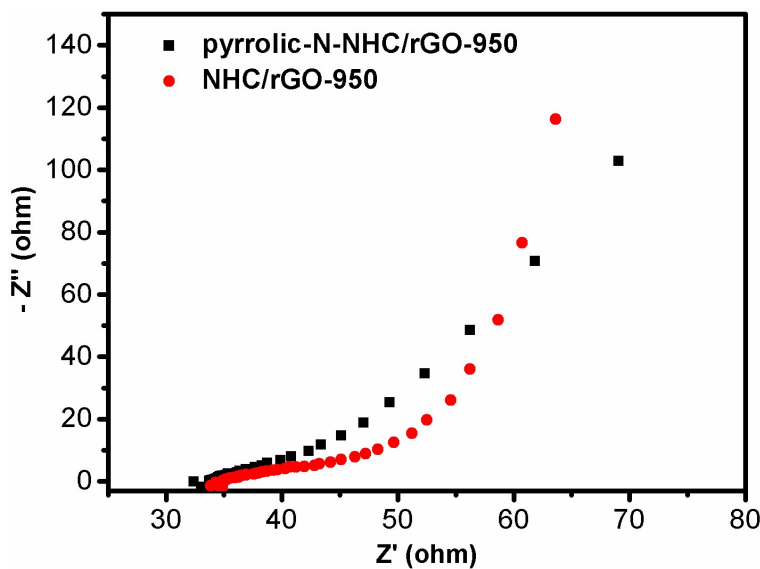


**Fig. S17.** Nyquist plots of electrochemical impedance spectra for pyrrolic-N-NHC/rGO-950 in 0.1 M KOH.

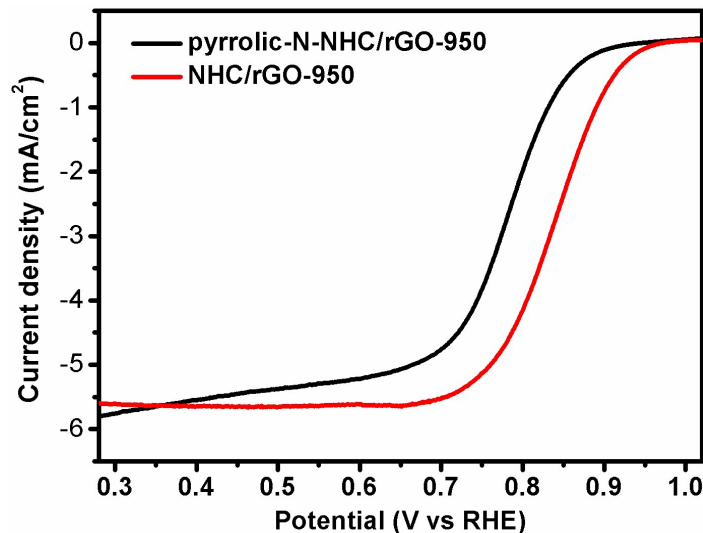


**Fig. S18.** LSV curves of pyrrolic-N-NHC/rGO-950 in  $O_2$ -saturated 0.1 M KOH solution at a rotation speed of 1600 rpm.

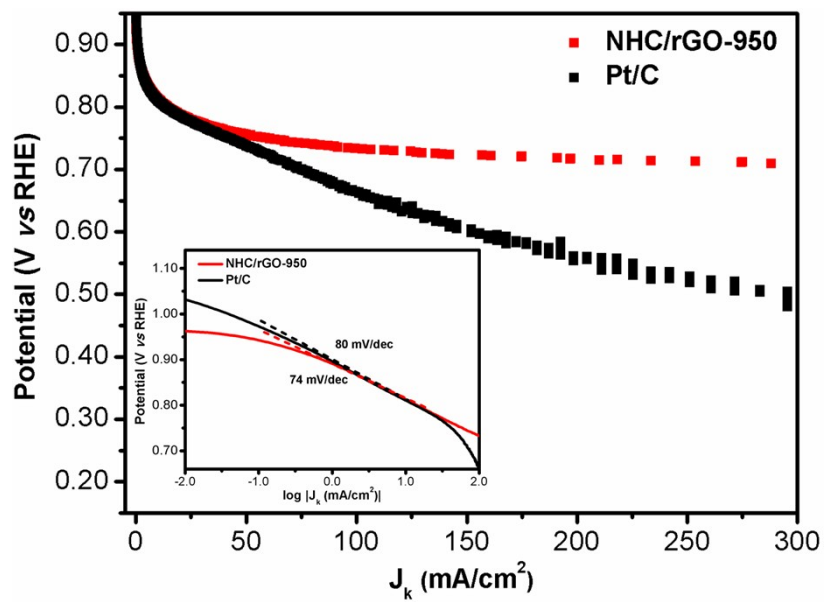


**Fig. S19.** Kinetic behavior of NHC/rGO-950 and Pt/C (inset: Tafel plots of NHC/rGO-950 and Pt/C).

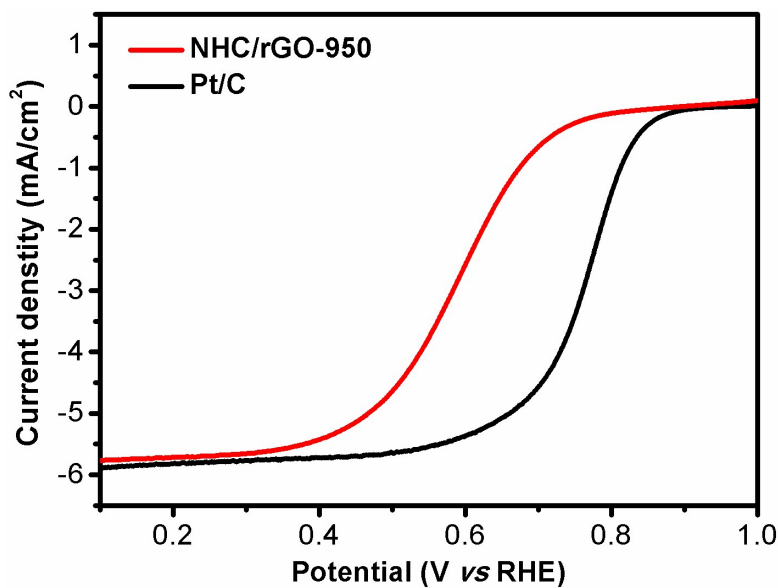


**Fig. S20.** LSV curves of NHC/rGO-950 in  $\text{O}_2$ -saturated 0.1 M  $\text{HClO}_4$  solution at a rotation speed of 1600 rpm.

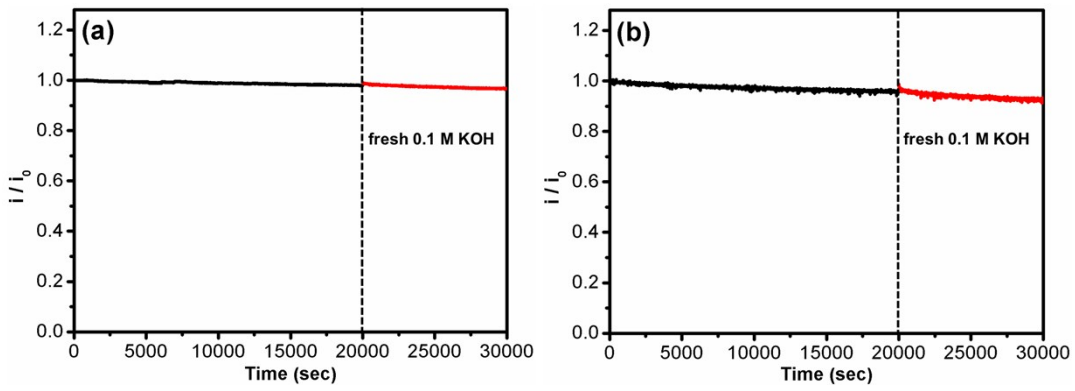


**Fig. S21.** Time-dependent current density curves for (a) NHC/rGO-950 and (b) Pt/C in 20000s and restarting the electrocatalytic test in a fresh portion of the 0.1 M KOH for another 10000s.

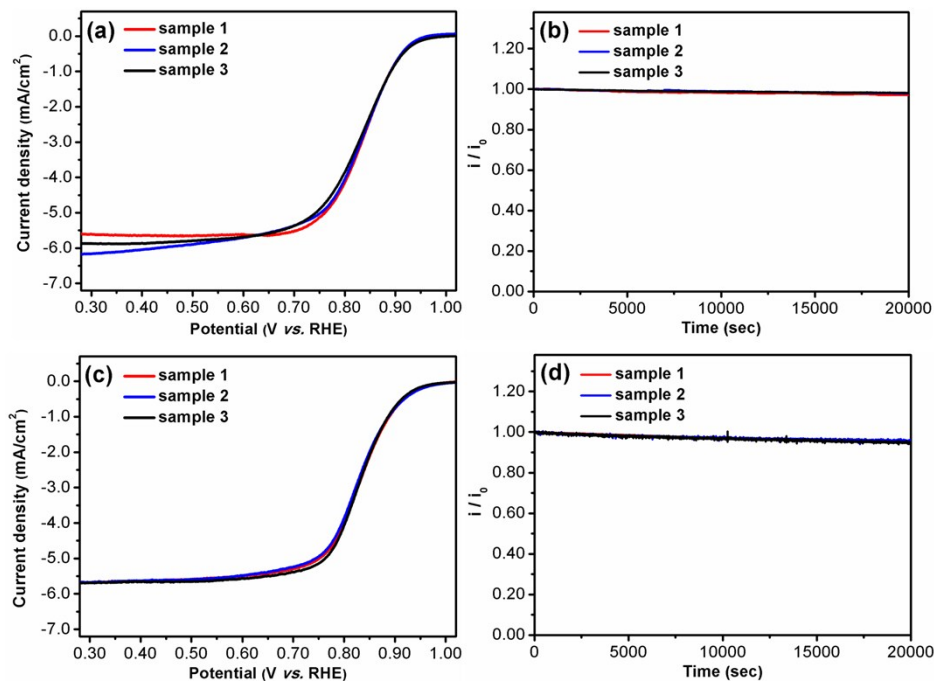


**Fig. S22.** The reproducibility of (a) LSV curves and (b) time-dependent current density curves for NHC/rGO-950. The reproducibility of (c) LSV curves and (d) time-dependent current density curves for Pt/C. The slightly larger curve deviation in (a) should be caused by three batches of the NHC/rGO-950 catalyst.

**Table S1.** Elemental analysis of N for different samples.

Sample	NHC-950	NHC/rGO-950	NHC/rGO-850	NHC/rGO-1050	pyrrolic-N- NHC/rGO-950
N [%]	1.64	1.58	1.72	1.28	1.74

**Table S2.** Comparison of ORR performance for NHC/rGO-950 with other metal-free electrocatalysts or Pt-based reference catalysts in 0.1 M KOH solution.

Catalyst	Half-wave potential (V vs RHE)	Tafel slope (mV/dec)	Kinetic current at 0.8 V (mA/cm <sup>2</sup> )	Mass activity at 0.8 V (mA/mg)	Reference
NHC/rGO-950	0.83	74	14.45	51.6 <sup>a</sup>	This work
g-C <sub>3</sub> N <sub>4</sub> @CMK-3	0.76	113	1.52	17.9 <sup>a</sup>	<i>J. Am. Chem. Soc.</i> 2011, <b>133</b> , 20116
G-CN800	0.76	--	3.08	44 <sup>a</sup>	<i>Angew. Chem. Int. Ed.</i> 2011, <b>50</b> , 5339
NGS-H	0.75	--	1.70	56.7 <sup>a</sup>	<i>J. Power Sources</i> 2011, <b>196</b> , 9970
Mesoporous N-Carbon	0.79	--	5.4	8.2 <sup>a</sup>	<i>J. Am. Chem. Soc.</i> 2011, <b>133</b> , 206
POMC-3	0.76	--	6.5	8.2 <sup>a</sup>	<i>J. Am. Chem. Soc.</i> 2012, <b>134</b> , 16127
P, N-CNT	0.75	--	3.0	37.5 <sup>a</sup>	<i>J. Phys. Chem. Lett.</i> 2012, <b>3</b> , 2863
PDMC800°C	0.73	--	0.70	7 <sup>a</sup>	<i>J. Am. Chem. Soc.</i> 2013, <b>135</b> , 7823
NG-1000	0.82	--	12.77	45.1 <sup>a</sup>	<i>ACS Appl. Mater. Interfaces</i> 2013, <b>5</b> , 11108
GNPCSS-800	0.81	--	13.43	67.2 <sup>a</sup>	<i>Angew. Chem. Int. Ed.</i> 2014, <b>53</b> , 14235
Carbon-L	0.69	--	0.55	5.5 <sup>a</sup>	<i>Energy Environ. Sci.</i> 2014, <b>7</b> , 442
GFMC3	0.8	--	1.93	7.6 <sup>a</sup>	<i>Phys. Chem. Chem. Phys.</i> 2014, <b>16</b> , 4251
HCH-dca-900 (r = 1.0)	0.71	--	1.21	2.6 <sup>a</sup>	<i>J. Mater. Chem. A</i> 2014, <b>2</b> , 605
meso/micro-PoPD	0.85		17.9	179 <sup>a</sup>	<i>Nat. commun.</i> 2014, <b>5</b> , 4973
CNT/HDC-1000	0.82	68	8.3	13.8 <sup>a</sup>	<i>Angew. Chem. Int. Ed.</i> 2014, <b>53</b> , 4102
ING	0.79	83	2.50	5 <sup>a</sup>	<i>Carbon</i> 2015, <b>95</b> , 930
P-CHS-2	0.77	--	4.59	9.1 <sup>a</sup>	<i>Carbon</i> 2015, <b>82</b> , 562
TTF-F	0.77	--	3.22	10.7 <sup>a</sup>	<i>Adv. Mater.</i> 2015, <b>27</b> , 3190
NMCS-3	0.76	--	2.10	3 <sup>a</sup>	<i>Angew. Chem. Int. Ed.</i> 2015, <b>54</b> , 588
N-MCNs	0.78	--	3.12	7.8 <sup>a</sup>	<i>Angew. Chem. Int. Ed.</i> 2015, <b>54</b> , 15191
MPSA/GO-1000	0.82	--	12.43	41.4 <sup>a</sup>	<i>Angew. Chem. Int. Ed.</i> 2016, <b>55</b> , 2230
N-CNS-120	0.76	--	6.34	31.1 <sup>a</sup>	<i>Adv. Mater.</i> 2016, <b>28</b> , 5080
NGM	0.77	--	3	12 <sup>a</sup>	<i>Adv. Mater.</i> DOI:10.1002/adma.201601406
N,P-CGHNs	0.82	--	6.34	21.1 <sup>a</sup>	<i>Adv. Mater.</i> 2016, <b>28</b> , 4606

N/S-2DPC-60	0.75	--	1.70	6.8 <sup>a</sup>	<i>Adv. Funct. Mater.</i> DOI:10.1002/adfm. 201602158
NPC-F	0.84	--	13.43	56.0 <sup>a</sup>	<i>Adv. Mater.</i> 2016, <b>28</b> , 1981
PtCu	0.84	47	13.43	839.6 <sup>b</sup>	<i>J. Electrochem. Soc.</i> 2012, <b>159</b> , B444.
PtCu NFs	0.89	--	15.11	1056 <sup>b</sup>	<i>Adv. Mater.</i> 2016, <b>28</b> , 8712
<b>Pt/C</b>	<b>0.83</b>	<b>80</b>	<b>13.49</b>	<b>134.9<sup>a</sup></b>	<b>This work</b>

<sup>a</sup> mass activity is calculated by the mass of total catalyst

<sup>b</sup> mass activity is calculated by the mass of Pt.

**Table S3.** ICP analysis for NHC/rGO-950 before and after reation.

Sample	Fe	Co	Pt	Zn
Before reaction	20 ppm	18 ppm	N.D.	N.D.
After reaction	10 ppm	16 ppm	N.D.	N.D.